RSC Advances

Facile synthesis and optical properties of pure and Ni^{2+}, Co^{2+}, Bi^{3+}, Sb^{3+} substituted Cu_3SnS_4.

Meenakshi Gusain, Pooja Rawat and Rajamani Nagarajan*

Materials Chemistry Group, Department of Chemistry, University of Delhi

Delhi 110007 INDIA

Abstract

Cu_3SnS_4 in orthorhombic symmetry has been stabilized by a simple and one pot synthesis involving the reaction of thiourea complexes of copper and tin. The obtained product has been characterized thoroughly using high resolution powder X-ray diffraction (PXRD), SEM-EDX, Raman, UV-Vis-NIR, and photoluminescence spectroscopy measurements. The presence of bands at 282, 317, 333 and 346 cm^{-1} in the Raman spectrum conclusively confirmed the orthorhombic symmetry of Cu_3SnS_4. Adopting this synthetic strategy, quaternary compositions consisting of nickel, cobalt, antimony and bismuth have been synthesized and characterized by all physico-chemical techniques. Of all these, compositions containing bismuth and antimony in place of tin are quite original and reported for the first time. While the nickel substitution retained the orthorhombic symmetry, cobalt substitution resulted in tetragonal symmetry of the quaternary composition. Similarly, the presence of bismuth ion in the lattice preserved the orthorhombic symmetry and the PXRD pattern of the product containing Sb^{3+}-ion could be indexed in tetragonal symmetry. Homogeneous distribution of all these elements in the samples was verified from scanning TEM technique. Band gap of pure and Ni^{2+}, Co^{2+}, Bi^{3+} and Sb^{3+}

*Corresponding author E-mail: rnagarajan@chemistry.du.ac.in

substituted Cu_3SnS_4 compositions, determined from the UV-Vis-NIR absorbance data, were in the range of 0.9- 1.46 eV. This is ideally suited for the use of these materials in photovoltaic cells.

1. Introduction

Band gap engineering in semiconductors to equip them for suitable applications has been extensively investigated.[1] Among chalcogenide based semiconductors, studies on the inexpensive, non-hazardous, non-toxic compositions of Cu-Sn-S are being conducted for energy related applications including solar cells.[2] The three known phases in Cu-Sn-S system, viz., Cu_2SnS_3, Cu_3SnS_4 and Cu_4SnS_4 possess structures derived from ZnS structure.[3] Owing to its suitable band gap, orthorhombic Cu_3SnS_4 can be a potential light absorption material for solar cells.[4] The enormous structural diversity shown by Cu_3SnS_4 offers enough opportunities for chemists to design new greener synthetic methodologies that are preferably one-step, without using toxic solvents, cheaper methods and simpler (easier) reaction conditions. In Cu_3SnS_4, hexagonally closed packed sulfur anionic network is present in which cations occupy half of the tetrahedral interstices. From the band structure calculations, the valence band maximum (VBM) of Cu_3SnS_4 has been estimated to consist of antibonding component of hybridization between Cu *d* states and S *p* states, while the conduction band minimum (CBM) included mainly the antibonding component of hybridization between Sn *s* and S *s* states.[5] This distinction is quite advantageous to tune the band gap by substituting with suitable cations either at the copper site or at the tin site in Cu_3SnS_4. Incorporation of fourth metal ion into Cu_3SnS_4 system leads to the quaternary compositions Cu_2MSnS_4 showing ideal absorption characteristics in the visible region to be used in solar cells.[6-8] For example, by the appropriate choice of fourth metal ion, one can impart additional optical, photochemical, thermoelectric and magnetic functions.[7, 8] The structural flexibility offered by quaternary compositions provides additional advantage to engineer them for suitable applications. Considering Cu_3SnS_4 as Cu_2CuSnS_4, replacing the copper with other transition metal ions such as Co^{2+}, Ni^{2+}, Fe^{2+} and Zn^{2+} resulting in quaternary compositions Cu_2MSnS_4 have been attempted.[9] Cu_2CoSnS_4 (CCTS) has been fabricated in all the three different arrangements of zincblende (cubic), tetragonal and wurtzite (hexagonal) by following solution based synthetic routes (solvothermal approach) with and without the use of surfactants.[9(a), 10] As compared to CCTS, very few literature reports exist on the successful synthesis of Cu_2NiSnS_4 (CNTS) and their properties. While wurtzite arrangement resulted CNTS from the solvothermal reaction of CuCl, $SnCl_2.2H_2O$ $Ni(NO_3)_2.6H_2O$ and 3-mercaptopropanoic acid in a coordinating solvent hexylamine,[9(a)] zincblende form was obtained when the sulfur source and the solvent changed to thiourea and ethyleneglycol, respectively.[8(b)] The variations in the symmetry of final products demonstrated the complex relation between the nature of reactants, nature of solvent and the mode of synthesis in addition to the challenge of preventing the formation of thermodynamically stable binary sulfides.[8(b), 9-13] Metal-thiourea precursors have been demonstrated to be versatile in generating not only various compositions of Cu-S system but also in stabilizing metastable ternary phases of $CuInS_2$ and $CuFeS_2$ in ethyleneglycol.[14] The present study is aimed to generate Ni^{2+}, Co^{2+} (transition metals) substituted for Cu^{2+}-ions and Bi^{3+} and Sb^{3+} (*p*-block elements) substituted for Sn^{4+} of Cu_3SnS_4 by a simple, one step procedure in a less coordinate solvent (ethyleneglycol) with the simultaneous understanding of their role on the choice of symmetry, structure and the optical properties of the final products. The obtained results are discussed below.

2. Experimental

2.1 Synthesis of precursors

(i) Synthesis of $[Cu(tu)_3]Cl$

$[Cu(tu)_3]Cl$ was obtained by reacting 0.099 g (1 *mmol*) of freshly prepared CuCl with 5 mL aqueous solution containing 0.2284 g (3 *mmol*) of thiourea (Spectrochem, 98%) under constant stirring over a period of 30 minutes.[15] After the reaction, the solution was filtered to remove any unreacted solid and crystallized at room temperature. To get the sufficient quantity of the complex, the reaction was repeated several times.

(ii) Synthesis of [Sn(tu)]Cl$_2$

1.1282 g of $SnCl_2.2H_2O$ (Sigma Aldrich, 99.99 %) was dissolved in a minimum amount of 5 M HCl solution. A solution of thiourea (0.3806 g in 10 ml) was added drop wise to $SnCl_2.2H_2O$ solution under constant stirring.[16] The complex formed was dried naturally.

(iii) Synthesis of [Ni(tu)$_4$]SO$_4$

1.1417 g of thiourea was dissolved in a minimum amount of water (15 ml) under constant stirring over a magnetic stirrer. To a 10 ml aqueous solution containing 1.3137 g of nickel (II) sulfate (Qualigens, AR Grade), thiourea solution was added drop wise under constant stirring and continued for 1 h.[17] After evaporation, the green colored crystals were collected.

(iv) Synthesis of [Co(tu)$_2$]Cl$_2$

0.7612 g of thiourea was dissolved in a minimum amount of water (15 ml) with constant stirring over a magnetic stirrer. To a 10 ml aqueous solution containing 1.1896 g of cobalt (II) chloride (CDH, 99%), thiourea solution was added drop wise under constant stirring. The reaction was continued for 1 h, after which, blue colored crystals were obtained.[18, 19]

(v) Synthesis of [Bi$_3$(tu)$_3$]Cl$_3$

2.3298 g of bismuth oxide (Bi_2O_3, Sigma Aldrich, 99.99 %) was dissolved in 20 ml of 5 M HCl, to which 10 ml aqueous solution containing 1.5224 g of thiourea was added drop wise.[20] The reaction mixture was stirred for 3 h and transferred to a petri dish and evaporated.

(vi) Synthesis of $[Sb(tu)_2]Cl_3$

1.4576 g of antimony oxide (Sb_2O_3, Sigma Aldrich, 99.99 %) was dissolved in 20 ml of 5 M HCl, to which 10 ml aqueous solution containing 1.5224 g of thiourea was added drop wise. After stirring for 3 h at room temperature, the complex was transferred and dried in a petri dish.[21]

2.2 Synthesis of Cu-M-Sn-S compositions

0.9825 g of $[Cu(tu)_3]Cl$ (3 *mmol*) and 0.2651g of $[Sn(tu)]Cl_2$ (1 *mmol*) were mixed well in the solid state to which in 50 ml of ethyleneglycol (Merck, AR Grade) was added. Within few minutes of refluxing, the solution turned brown in colour. But the reaction was continued for 1.5 h. The product after the reaction was separated by centrifugation and washed repeatedly with double distilled water, ethanol and carbon disulphide. The sample was dried naturally at room temperature. Ni^{2+}, Co^{2+}, Bi^{3+} and Sb^{3+} substitutions were attempted by simple refluxing of 0.4592 g (1 *mmol*) $[Ni(tu)_4]SO_4$ / 0.2865 g (1 *mmol*) $[Co(tu)_2]Cl_2$/ 0.3208 g (0.33 *mmol*) $[Bi_3(tu)_3]Cl_3$/ 0.3806 g (1 *mmol*) $[Sb(tu)_2]Cl_3$ with 0.6548 g (2 *mmol*) of $[Cu(tu)_3]Cl$ and 0.2651 g (1 *mmol*) of $[Sn(tu)]Cl_2$ in 50 ml of ethyleneglycol for 3 h. The product was separated by centrifugation, washed with double distilled water followed by ethanol and carbon disulfide.

2.3 Characterization

Powder X-ray diffraction (PXRD) patterns were recorded using PANalytical Empyrean diffractometer, equipped with PIXcel^{3D} detector, employing Cu K_α radiation (λ = 1.5418 Å) with scan step size of 0.01313° and 188.44 seconds/step. UV-Vis-NIR absorbance spectra of the samples were collected using a Thermo Scientific UV-Vis-NIR spectrophotometer (Model Evolution 300) equipped with an integrating sphere by dispersing them in *n*-hexane. Raman spectrum in compact form was collected using a Renishaw via Microscope system with a diode laser (λ = 785 nm). Transmission Electron Microscopy (TEM) and Selected Area Electron

Diffraction (SAED) were carried out on an FEI Technai G^2 30 electron microscope operating at 300 kV. Scanning electron microscopic (SEM) images were captured using a Zeiss EVO 50 microscope and FE-SEM Quanta 200 FEG microscope equipped with EDS detector. Elemental mapping of the samples was surveyed with JEOL 6610LV Scanning Electron Microscope. Photoluminescence spectroscopy measurements were carried out on the Horiba Jobin Yuvon Fluorolog- 3 modular spectrofluorometer at room temperature employing CW xenon lamp source on solid samples using front side and right angle detection configuration.

3. Results and Discussion

As metal- thiourea complexes have been used as the starting materials, their formations have been confirmed from FTIR, Raman spectroscopic analysis. The positions of FTIR bands of the reaction of one mole of CuCl with three moles of thiourea were present at 1477, 1389, 1093 and 710 cm^{-1} showing significant change from the position of bands for free thiourea (1473 (ν(CN)), 1414 (ν(CS)), 1083 (ν(CN)) and 730 cm^{-1} (ν(CS))) (Fig. S1 ESI†).[15] In the Raman spectrum, bands at 150, 200, 420, 475 and 707 cm^{-1} were present suggesting the formation of complex in 1:3 between CuCl and thiourea.[22] The presence of characteristic bands in the FT-IR and Raman spectra indicated the formation of 1:1 complex of $SnCl_2.2H_2O$ and thiourea (Fig. S2 ESI†).[16] Similarly, complex formation between $NiSO_4.6H_2O$ and thiourea in 1:4 stoichiometry was confirmed from its finger print positions (478 cm^{-1} and 734 cm^{-1}) in the Raman spectrum (Fig.S3 ESI†).[17] Similar confirmation for the 1:2 complex between $CoCl_2.6H_2O$ and thiourea was sought from its Raman spectrum (Fig.S4 ESI†).[19] While both FT-IR and Raman spectra confirmed the formation of $[Sb(tu)_2]Cl_3$, band positions at at 1623, 1379, 1094 and 693 cm^{-1} in the FT-IR spectrum indicated the formation of $[Bi_3(tu)_3]Cl_3$ (Fig.S5 and S6 ESI†).[20, 21]

PXRD pattern of the solid product from the reaction of copper and tin thiourea complexes is presented in Fig. 1(a) (i). All the observed reflections could be indexed in an orthorhombic unit cell with a = 6.787 (44) Å, b = 7.728 (78) Å and c = 37.555 (33) Å. These values are close to the reported values in the JCPDS file no 36-0217. The average crystallite size (D) of the sample, estimated from the Scherrer analysis was 3 nm. Uniform spherical morphology was observed across the analyzed area of the sample by SEM. Ratio of Cu, Sn and S from EDX analysis was as 3.1: 0.9: 4, closer to the composition of Cu_3SnS_4 (Fig. S7 ESI†). The presence of bands at 282, 317, 333 and 346 cm^{-1} in the Raman spectrum conclusively confirmed the orthorhombic symmetry of Cu_3SnS_4 (Fig. 2(a)).[4, 23] The sample showed absorption in whole of the visible range in the UV-Vis-NIR absorption spectrum and the Tauc plot ($(\alpha h\nu)^2$ versus $h\nu$), yielded a band gap of 1.21 eV (Fig. 2(b) and Fig. 2(c)). This is less than the theoretically calculated value of 1.6 eV.[4] This deviation might be due to quantum confinement arising from the nanosized crystallites. When excited with 270 nm, Cu_3SnS_4 showed two emission bands at 417 and 439 nm respectively (Fig. 2(d)). Band at 439 nm might be the electron hole recombination band and the one at 417 nm might be arising from $3d^9\,4s^1 \leftrightarrow 3d^{10}$ transition of Cu^+ ion.[24, 25]

PXRD pattern of the product, from the reaction of thiourea complexes of copper, nickel and tin is presented in Fig. 1 (a) (ii). It showed close resemblance to the PXRD pattern of orthorhombic Cu_3SnS_4 with the observed reflections showing no significant shift in the two-theta positions. From the Le Bail refinement, the determined lattice constants were a = 6.581 (18) Å, b = 8.104 (31) Å and c = 37.754 (95) Å. Incorporation of Ni^{2+} for Cu^{2+} in Cu_3SnS_4 was not clear from PXRD results. Use of other techniques, such as STEM, Raman spectroscopy and SEM-EDX analysis was sought for the verification of uniform inclusion of nickel in Cu_3SnS_4. The ratio between Cu: Ni: Sn: S, from EDX analysis was 2.5: 0.9: 0.9: 3.7 (Fig. S8 ESI†). STEM-

HAADF image and corresponding EDS elemental maps (shown in Fig. 1 (b)) depicted homogeneous distribution of the four elements in the sample. The scanning SEM images also validated the homogeneity of the sample at micro-crystalline level (Fig. S9 ESI†). Raman spectrum of nickel substituted Cu_3SnS_4 is shown in Fig. 2(a) in which peak broadening is observed arising from the phonon confinement. It was deconvoluted to yield three peaks at 282, 311 and 348 cm^{-1} (Fig. 2(a)). In the UV-Vis-NIR spectrum, a broad band starting from visible region and extending up to infra-red region was observed for the sample (Fig. 2(b)). Estimated band gap from the Tauc plot was 1.46 eV, higher than the value observed for Cu_3SnS_4 (Fig. 2(c)). Single broad emission occurring in the ultraviolet region was noticed in the PL spectrum on exciting it with λ = 270 nm (Fig. 2(d)). As noted earlier, this could be a recombination band.[24] SAED patterns of this phase are displayed in Fig. S10 (ESI†). The observed spots in the SAED pattern could be indexed to orthorhombic unit cell corresponding to [20$\underline{20}$], [20$\underline{12}$], [00$\underline{12}$] and [00$\underline{10}$] *hkl* planes.

In Fig. 3(a), PXRD pattern of the product from the reaction of Cu-Co-Sn-tu complexes in 2: 1: 1 molar ratio is presented. All the observed reflections could be indexed in tetragonal symmetry following the JCPDS card no. 26-0513 with the composition, Cu_2CoSnS_4. The lattice constants from the Le Bail refinement were a = 5.471 (13) Å and c = 11.663 (51) Å. EDX analysis confirmed the presence of cobalt in the samples yielding a ratio of 2.4: 0.6: 0.7: 4.2 for Cu: Co: Sn: S (Fig. S11 ESI†). Elemental mapping confirmed the uniform presence of all the constituent elements across the cross-section of samples (Fig. 3(b)). Room temperature Raman spectrum of this sample is shown in Fig. 4(a). On deconvolution, bands at 288, 320 and 347 cm^{-1} have been observed. Band positions were matching well with earlier reports.[10 (a)] Fig. 4(b) represents UV-Vis-NIR absorbance spectrum of Co-substituted Cu_3SnS_4 with absorption edge near 900 nm. The estimated band gap value was 1.23 eV (Fig. 4(c)). Photoluminescence emission spectrum, obtained using excitation wavelength of 270 nm, showed a small hump at 330 nm arising from the Co^{2+}-ion in the tetrahedral coordination with sulphur (Fig. 4(d)).[26] This feature also conclusively confirmed the introduction of cobalt in Cu-Sn-S network.

We extended our success of synthesizing quaternary phases, to generate novel compositions consisting of other *p*-block elements. PXRD pattern from the reaction of thiourea complexes of copper, tin and bismuth is shown in Fig. 5(a). Using auto indexing program TREOR, all the observed reflections could be indexed in an orthorhombic symmetry with a = 6.833 (12) Å, b = 8.153 (15) Å and c = 38.889 (89) Å. The observed parameters were slightly higher than the values of Cu_3SnS_4 hinting possible substitution of larger Bi^{3+}-ion (0.103 nm) for some of the relatively smaller Sn^{4+}-ions (0.055 nm). Flower like morphology was noticed for the samples in its SEM images (Fig S11 ESI†). EDX analysis, performed at various locations of the sample, indicated the uniform presence of bismuth in the samples in addition to copper, tin and sulfur. From the analysis, the obtained ratio of Cu: Bi: Sn: S was 2.9: 0.4: 1.0: 3.7. Elemental mapping also confirmed the homogeneous distribution of the elements in the samples (Fig. 5(b)). In the Raman spectrum of Bi^{3+} substituted Cu_3SnS_4, three bands at 290, 316 and 347 cm^{-1} were observed as against four for Cu_3SnS_4. The absence of most intense band at 333 cm^{-1}, a typical feature noticed in Cu_3SnS_4, suggested the change in the vibration mode of Sn-S by the substitution of bismuth (Fig. 6(a)). Broad absorbance over the entire range of visible region with band edge near 950 nm was observed in the UV-Vis-NIR spectrum of Bi^{3+}-substituted sample (Fig. 6(b)). Band gap from the Tauc plot was 1.21 eV (Fig. 6(c)). Emission maxima shifted from 342 nm (for Cu_3SnS_4) to 315 nm (for Bi-substituted sample) and this could possibly due to $^3P_{0,1} \rightarrow {}^1S_0$ transition of Bi^{3+} -ion (Fig. 6(d)).[27]

Fig. 7 (a) shows the PXRD pattern of the product resulted from our attempts to include Sb^{3+} in Cu_3SnS_4 lattice. The diffraction pattern resembled closely with the one for Cu_2CoSnS_4. The pattern could very well be indexed in tetragonal symmetry (*I-42m* space group) with lattice constants, a = 5.395 (95) Å and c = 11.429 (24) Å. To appreciate the finer distinctions between the synthesized compositions, the indexed parameters used for their PXRD patterns, the band gap values, Raman band positions and the emission band positions in the PL spectra have been compiled in Table 1 and 2, respectively. Flower like morphology was seen uniformly throughout the scanned area in the SEM images of the Sb^{3+} containing sample. EDX analysis at various locations yielded ratio of 3.1: 0.3: 0.9: 3.7 for Cu: Sb: Sn: S (Fig. S11 ESI†). Also, elemental mapping by SEM-EDX analysis confirmed the homogeneous distribution of constituent elements of the sample (Fig. 7(b)). Raman spectrum of this sample is shown in Fig. 8(a). Three bands centered at 282, 314 and 348 cm^{-1} could be located after deconvolution (Fig. 8(a)). Observed bands were anti-stoke shifted from the positions observed for Cu_2CoSnS_4. Band gap of 0.99 eV was estimated from UV-Vis-NIR spectral data (Fig. 8(b) and Fig. 8(c)). When excited with 270 nm, emission at 342 nm was observed. Observed emission could be assigned to the transition of spin forbidden relaxation $^3P_1$-^1S_o of Sb^{3+}-ion (ns^2 type) (Fig. 8(d)).[28]

4. Conclusions

A simple, reliable, rapid and low-cost synthetic method has been developed for the photovoltaic material, Cu_3SnS_4 in orthorhombic symmetry. The structure, symmetry and homogenous distribution of the constituents have been verified from diffraction, spectroscopy and microscopy techniques. Optical band gap of Cu_3SnS_4, estimated from the UV-Vis-NIR spectroscopy data, was 1.21 eV. Substituting Cu_3SnS_4 with *d*-block ions (Ni^{2+}, Co^{2+}) and *p*- block ions (Bi^{3+}, Sb^{3+}) resulted in either variation in the symmetry and/or the optical band gap values in the range, ideally suited for photovoltaic applications. The philosophy of these sets of reactions has the potential to generate new compositions in other ternary and quaternary compositions.

Essential Supporting Information (ESI†)

FTIR and Raman spectrum of precursors, SEM-EDX of Cu_3SnS_4, SEM image, EDX spectrum, SAED pattern and elemental mapping of Cu_2NiSnS_4, SEM-EDX of Cu_3SnS_4, nickel, cobalt, bismuth and antimony substituted Cu_3SnS_4.See DOI: 10.1039/b000000x/.

Acknowledgements

Authors wish to record their sincere thanks to DST (Nanomission) and DST (SB/S1/PC-08/2012) for funding this research. MG and PR thanks CSIR, New Delhi and DST respectively for their fellowship. Thanks are due to University of Delhi, Delhi for the usage of facilities of CIF, M.Tech (NSNT) program.

References

1 (a) F. Capasso and A.Y. Cho, *Surf. Sci.* 1994, **299-300**, 878. (b) F. Capasso, *Science* 1987, **235**, 172.

2 (a) C.Z. Wu, Z.P. Hu, C. Wang, H. Sheng, J. Yang and Y. Yie, *Appl. Phys. Lett*. 2007, **91**, 143104. (b) B. Li, Y. Xie, J. Huang and Y. Qian, *J Solid State Chem*. 2000, **153**, 170. (c) J. Xu, X. Yang, T.L. Wong and C.S. Lee, *Nanoscale* 2012, **4**, 6537.

3 (a) X.A. Chen, H. Wada, A. Sato and M. Mieno, *J. Solid. State Chem.* 1998, **139**, 144. (b) X.A. Chen, H. Wada and A. Sato, *Mater. Res. Bull.* 1999, **34**, 239. (c) P.S. Jaulmes, J. Rivet and P. Laruelle, *Acta Crystallogr. B* 1977, **33**, 540. (d) P.S. Jaulmes, M. Julien-Pouzol, J. Rivet, J.C. Jumas and M. Maurin, *Acta Crystallogr. B* 1982, **38**, 51.

4 P.A. Fernandes, P.M.P. Salome and A.F. da Cunha, *J. Phys D: Appl Phys* 2010, **43**, 215403.

5 Y.T. Zhai, S. Chen, J.H. Yang, H.J. Xiang, X.G. Gong, A. Walsh, J. Kang and S.H. Wei, *Phys. Rev. B* 2011, **84**, 075213.

6 (a) D.B. Mitzi, O. Gunawan, T.K. Todorov, K. Wang and S. Guha, *Sol. Energy Mater. Sol. Cells* 2011, **95**, 1421. (b) B. Murali, M. Madhuri and S.B. Krupanidhi, *Cryst. Growth Des.* 2014, **14**, 3685.

7 (a) L. Shi and Y. Li, *RSC Adv.* 2014, **4**, 43720. (b) H. Yang, L.A. Jauregui, G. Zhang, Y.P. Chen and Y. Wu, *Nano Lett.* 2012, **12**, 540. (c) G. Nenert and T.T.M. Palstra, *J. Phys.: Condens. Matter* 2009, **21**, 176002. (d) L. Shi, Y. Li, H. Zhu and Q. Li, *Chem. Plus Chem.* 2014, **79**, 1638.

8 (a) X. Zhang, N. Bao, B. Lin and A. Gupta, *Nanotechonolgy* 2013, **24**, 105706. (b) T.X. Wang, Y.G. Li, H.R. Liu, H. Li and S.X. Chen, *Mater. Lett.* 2014, **124**, 148.

9 (a) Y. Cui, R. Deng, G. Wang and D. Pan, *J Mater Chem.* 2012, **22**, 23136. (b) D. Aldakov, A. Lefrancois and P. Reiss, *J Mater Chem.* 2013, **1**, 3756.

10 (a) J.Y. Chane-Ching, A. Gillorin, O. Zaberca, A. Balocchi and X. Marie, *Chem. Commun.* 2011, **47**, 5229. (b) A. Gillorin, A. Balocchi, X. Marie, P. Dufour and J.Y. Chane-Ching, *J. Mater. Chem.* 2011, **21**, 5615. (c) B. Murali and S.B. Krupanidhi, *J. Appl Phys.* 2013, **114**, 144312. (d) M. Benchikri, O. Zaberca, R.E. Ouatib, B. Durand, F. Oftinger, A. Balocchi and J.Y. Chane-Ching, *Mater Lett.* 2012, **68**, 340.

11 (a) C. Yan, C. Huang, J. Yang, F. Liu, J. Liu, Y. Lai, J. Li and Y. Liu, *Chem. Commun*. 2012, **48**, 2603. (b) X. Zhang, N. Bao, K. Ramasamy, Y.H.A. Wang, Y. Wang, B. Lin and A. Gupta, *Chem. Commun*. 2012, **48**, 4956. (c) Z. Gui, R. Fan, X. Chen, Y. Hu and Z. Wang, *Mater Res. Bull* 2004, **39**, 237. (d) A. Chaneschi, C. Cipriani, F. Di Benedetto and R. Sessoli, *Phys. Chem. Minerals* 2004, **31**, 190. (e) L. Li, X. Liu, J. Huang, M. Cao, S. Chen, Y. Shen and L. Wang,

Mater Chem Phys 2012, **133**, 688. (f) X. Jiang, W. Xu, R. Tan, W. Song and J. Chen, *Mater. Lett.* 2013, **102-103**, 39. (g) X. Liang, X. Wei and D. Pan, *J. Nanomaterials* 2012, ID 708648.

12 X. Liang, P. Guo, G. Wang, R. Deng, D. Pan and X. Wei, *RSC Adv.* 2012, **2**, 5044.

13 H. Guan, H. Shen, C. Gao and X. He, *J. Mater. Sci- Mater. Electron.* 2013, **24**, 1490.

14 (a) M. Gusain, P. Kumar and R. Nagarajan, *RSC Adv* 2013, **3**, 18863. (b) P. Kumar, S. Uma and R. Nagarajan, *Chem Commun* 2013, **49**, 7316.

15 P. Bombicz, I. Mutikainen, M. Krunks, T. Leskela, J. Madarasz and L. Niinisto, *Inorg. Chim. Acta*, 2004, **357**, 513.

16 J.E. Cassidy, W. Moser, J. D. Donaldson, A. Jelen and D.G. Nicholson, *J. Chem. Soc. (A)* 1970, 173**.**

17 A. Bhaskaran, C. M. Ragavan, R. Sankar, R. Mohankumar, and R. Jayavel, *Cryst. Res. Technol,* 2007, **42**, 477.

18 G. S. Murugan, N. Balamurugan, and P. Ramasamy, *Mater. Lett*. 2008, **62**, 3087.

19 S. Salama, H. Schugar and T.G. Spiro, *Inorg. Chem.* 1979, **18**, 10.

20 S.G. Bhat and S.M. Dharmaprakash, *Mater. Res. Bull.* 1998, **33**, 833.

21 I.I. Ozturk, N. Kourkoumelis, S. K. Hadjikakou, M.J. Manos, A.J. Tasiopoulos, I.S. Butler, J. Balzarini and N. Hadjiliadis, *J. Coord. Chem.* 2011, **6**, 3859.

22 P. Kumar, M. Gusain and R. Nagarajan, *Inorg. Chem.* 2011, **50**, 3065.

23 (a) P.A. Fernandes, P.M.P. Salome and A.F. da Cunha, *Phys. Status Solidi C* 2010, **3-4**, 901. (b) V.M. Dzhagan, A.P. Litvinchuk, M. Kruszynska, J. Kolny-Olesiak, M.Y. Valakh and D.R.T. Zahn, *J. Phys. Chem C* 2014, **118**, 27554.

24 H. Hu, Z. Liu, B. Yang, X. Chen, and Y. Qian, *J. Cryst. Growth* 2005, **284**, 226.

25 J.D. Barrie and B. Dunn, *J. Phys. Chem.* 1989, **93**, 3958.

26 S.-J Bao, Y. Li, C.M Li, Q. Bao, Q. Lu and J. Gao, *Cryst.Growth.Des.* 2008, **8**, 3745.

27 A.A. Setlur and A.M. Srivastava, *Opt. Mater.* 2006, **29**, 410.

28 F. Wen, J. Chen, J.-H. Moon, J.H. Kim, J. Niu and W. Li, *J. Solid State Chem.* 2004, **177**, 3114.

Figure Captions

Fig. 1 (a) PXRD pattern of (i) Cu_3SnS_4 (red) and (ii) Cu_2NiSnS_4 (blue) and (b) scanning TEM image of Cu_2NiSnS_4.

Fig. 2 (a) Raman spectrum (b) UV-Vis-NIR absorption spectrum (c) band gap estimation plot and (d) photoluminescence emission spectrum of Cu_3SnS_4 (red square) and Cu_2NiSnS_4 (blue circles) at λ_{exc} = 270 nm.

Fig. 3 (a) PXRD pattern and (b) scanning SEM image of Cu_2CoSnS_4.

Fig. 4 (a) Raman spectrum (b) UV-Vis-NIR absorption spectrum (c) band gap estimation plot and (d) photoluminescence emission spectrum of Cu_2CoSnS_4 at λ_{exc} = 270 nm.

Fig. 5 (a) PXRD pattern and (b) scanning SEM image of the sample obtained from the reaction to include Bi^{3+}- in Cu_3SnS_4.

Fig. 6 (a) Raman spectrum (b) UV-Vis-NIR absorption (c) band gap estimation plot and (d) photoluminescence emission spectrum of the sample obtained from the reaction to include Bi^{3+}- in Cu_3SnS_4 at λ_{exc} = 270 nm.

Fig. 7 (a) PXRD pattern and (b) scanning SEM image of the sample from the reaction to include Sb^{3+}- in Cu_3SnS_4.

Fig. 8 (a) Raman spectrum (b) UV-Vis-NIR absorption (c) band gap estimation plot and (d) photoluminescence emission spectrum of the sample from the reaction to include Sb^{3+}- in Cu_3SnS_4.

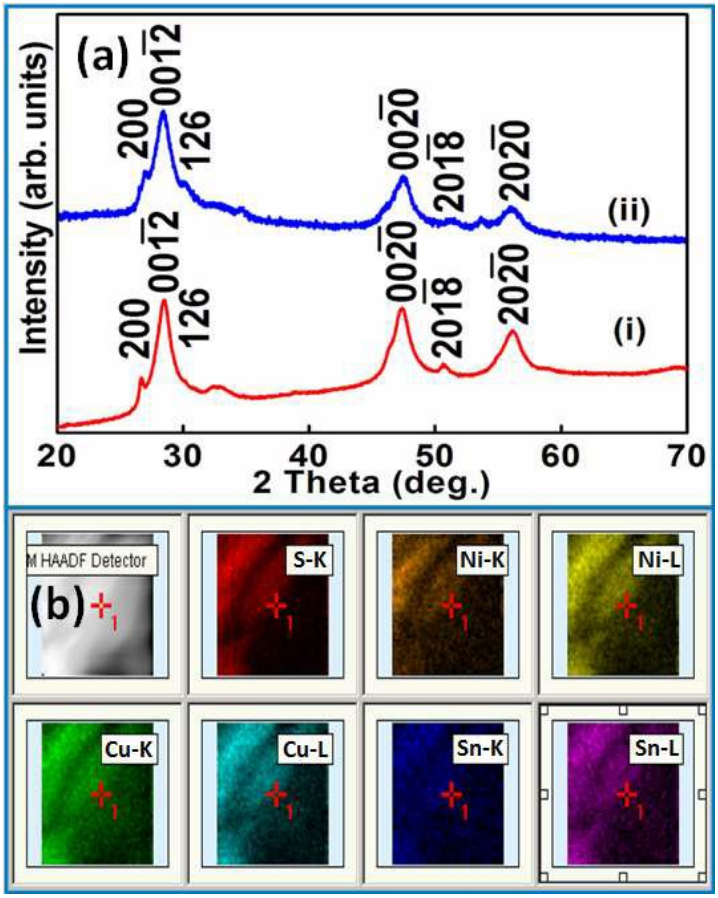

Fig. 1

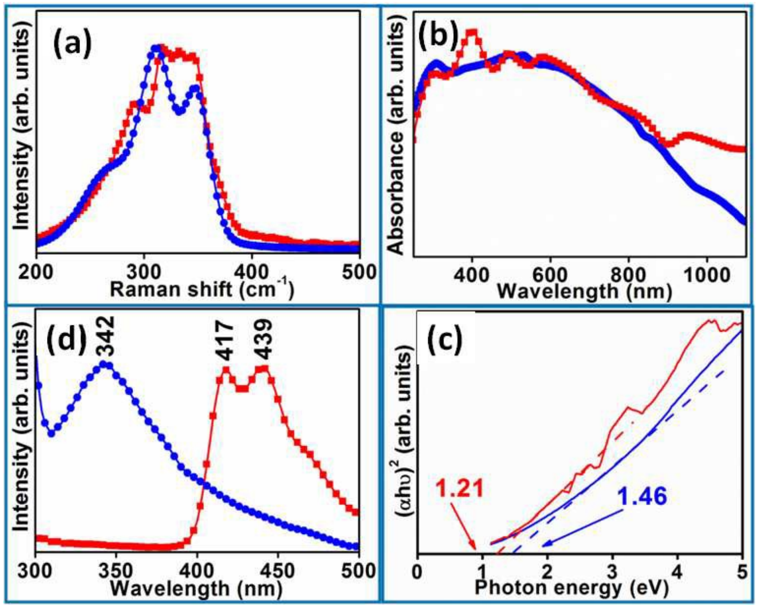
(a)
Intensity (arb. units)
Raman shift (cm^-1)
200
300
400
500
(b)
Absorbance (arb. units)
Wavelength (nm)
400
600
800
1000
(d)
342
417
439
Intensity (arb. units)
Wavelength (nm)
300
350
400
450
500
(c)
(αhυ)^2 (arb. units)
1.21
1.46
Photon energy (eV)
0
1
2
3
4
5

Fig. 2

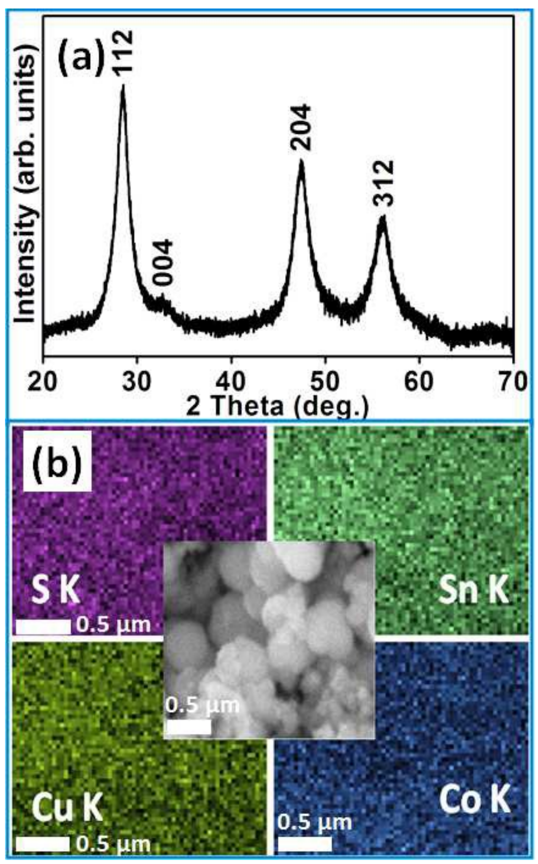
(a)
112
004
204
312
Intensity (arb. units)
2 Theta (deg.)
20
30
40
50
60
70
(b)
S K
0.5 µm
Sn K
0.5 µm
Cu K
0.5 µm
Co K
0.5 µm

Fig. 3

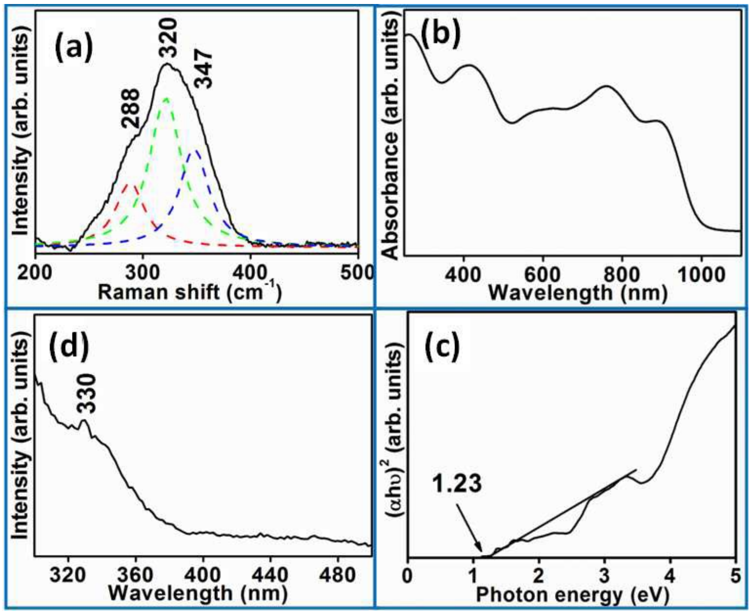
(a)
320
347
288
Intensity (arb. units)
Raman shift (cm^{-1})
200 300 400 500
(b)
Absorbance (arb. units)
Wavelength (nm)
400 600 800 1000
(d)
330
Intensity (arb. units)
Wavelength (nm)
320 360 400 440 480
(c)
$(\alpha h\upsilon)^2$ (arb. units)
1.23
Photon energy (eV)
0 1 2 3 4 5

Fig. 4

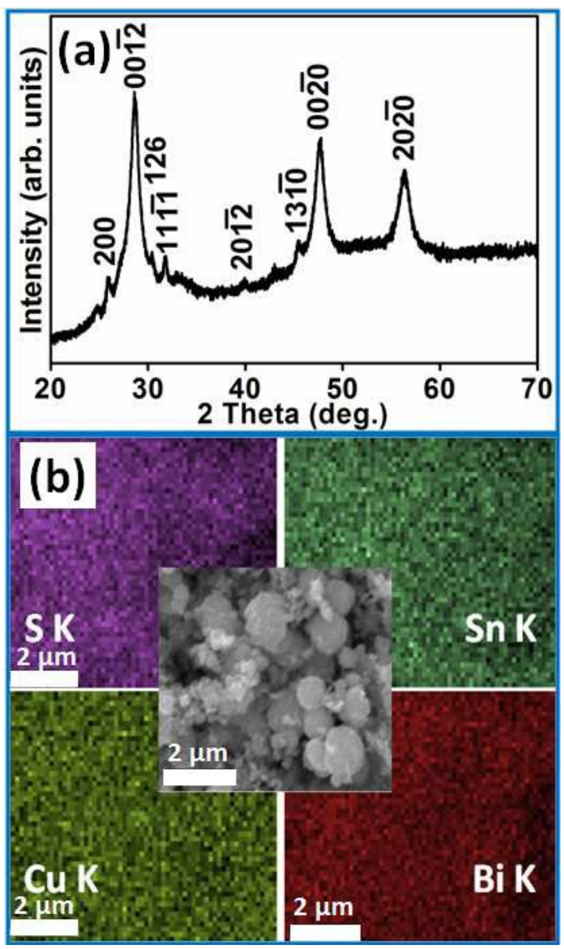
(a)
$00\bar{1}2$
200
$11\bar{1}\bar{1}$
126
$20\bar{1}2$
$13\bar{1}0$
$00\bar{2}0$
$20\bar{2}0$
Intensity (arb. units)
2 Theta (deg.)
20 30 40 50 60 70
(b)
S K
2 µm
Sn K
2 µm
Cu K
2 µm
Bi K
2 µm

Fig. 5

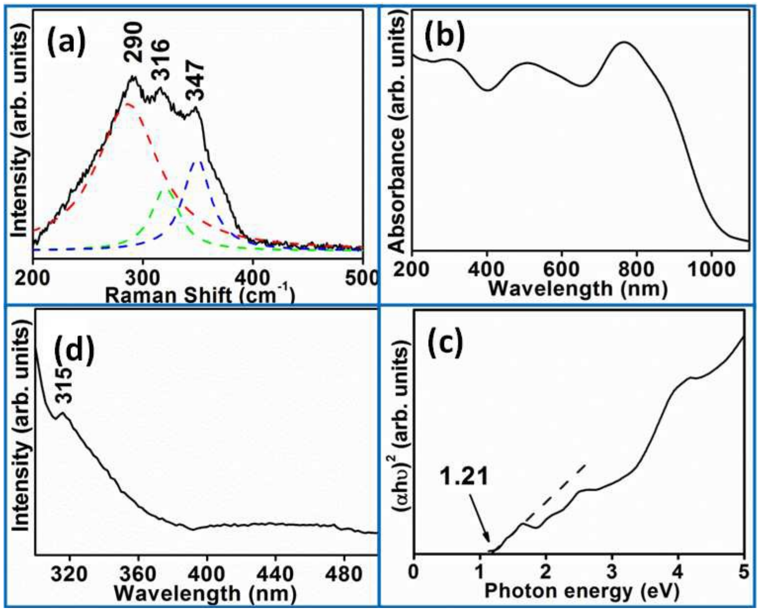
(a)
290
316
347
Intensity (arb. units)
Raman Shift (cm^{-1})
200
300
400
500
(b)
Absorbance (arb. units)
Wavelength (nm)
200
400
600
800
1000
(d)
315
Intensity (arb. units)
Wavelength (nm)
320
360
400
440
480
(c)
($\alpha h\upsilon$)^2 (arb. units)
1.21
Photon energy (eV)
0
1
2
3
4
5

Fig. 6

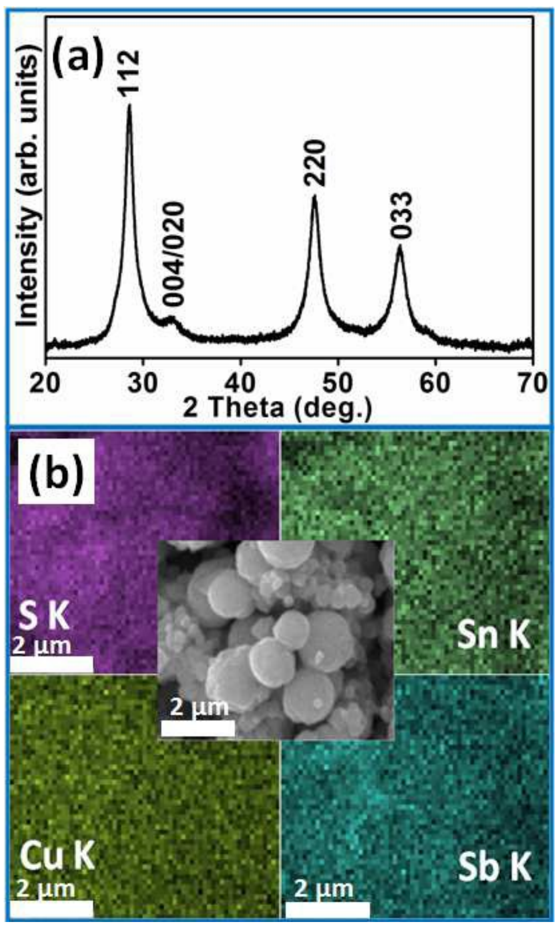
(a)
112
004/020
220
033
Intensity (arb. units)
2 Theta (deg.)
20
30
40
50
60
70
(b)
S K
2 µm
Sn K
2 µm
Cu K
2 µm
Sb K
2 µm

Fig. 7

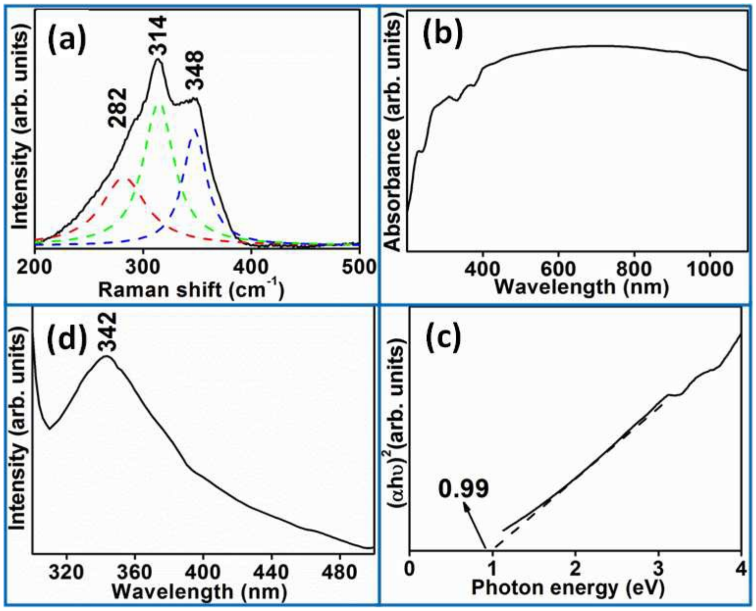
(a)
314
348
282
Intensity (arb. units)
200
300
400
500
Raman shift (cm^{-1})
(b)
Absorbance (arb. units)
400
600
800
1000
Wavelength (nm)
(d)
342
Intensity (arb. units)
320
360
400
440
480
Wavelength (nm)
(c)
$(\alpha h\upsilon)^2$(arb. units)
0.99
0
1
2
3
4
Photon energy (eV)

Fig. 8

Table 1 Crystallographic data of orthorhombic Cu_3SnS_4, Cu_2NiSnS_4, Cu_2BiSnS_4, Cu_2CoSnS_4 and Cu_2SbSnS_4.

Formula	**Cu_3SnS_4**	**Cu_2NiSnS_4**	**Cu_2BiSnS_4**	**Cu_2CoSnS_4**	**Cu_2SbSnS_4**
Crystal	Orthorhombic	Orthorhombic	Orthorhombic	Tetragonal	Tetragonal
Space	*Pmn2₁*	*Pmn2₁*	*Pmn2₁*	*I-42m*	*I-42m*
a [Å]	6.787 (44)	6.581 (18)	6.833 (12)	5.471 (13)	5.395 (95)
b [Å]	7.728 (78)	8.104 (31)	8.153 (15)	5.471 (13)	5.395 (95)
c [Å]	37.555 (33)	37.754 (95)	38.889 (89)	11.663 (51)	11.429 (24)
V [$Å^3$]	1970.09 (29)	2045.50 (11)	2166.76 (75)	349.10 (23)	332.76 (14)
R_{exp} (%)	0.77	1.54	1.73	1.15	3.13
R_p (%)	0.75	1.41	1.56	1.21	2.90
R_{wp} (%)	1.00	1.78	1.99	1.62	3.70
GoF	1.30	1.15	1.15	1.41	1.18
Step size	0.01313°	0.01313°	0.01313°	0.01313°	0.01313°
Temperature	298 K	298 K	298 K	298 K	298 K

Table 2 Summary of Raman, UV-Vis-NIR and photoluminescence spectral details of the compounds under the present study.

S.No.	**Composition**	**Raman band positions (cm^{-1})**	**Band gap from UV-Vis-NIR data (eV)**	**PL emission band positions (nm)**
1	Cu_3SnS_4	282, 317, 333, 346	1.21	417, 439
2	Cu_2NiSnS_4	282, 311, 348	1.46	342
3	Cu_2CoSnS_4	288, 320, 347	1.23	330
4	$Cu_2(Bi/Sn)S_4$	290, 316, 347	1.21	315
5	$Cu_2(Sb/Sn)S_4$	282, 314, 348	0.99	342

Facile synthesis and optical properties of pure and Ni^{2+}, Co^{2+}, Bi^{3+}, Sb^{3+} substituted Cu_3SnS_4.

Meenakshi Gusain, Pooja Rawat and Rajamani Nagarajan*

Materials Chemistry Group, Department of Chemistry, University of Delhi

Delhi 110007 INDIA

Essential Supporting Information (ESI†)

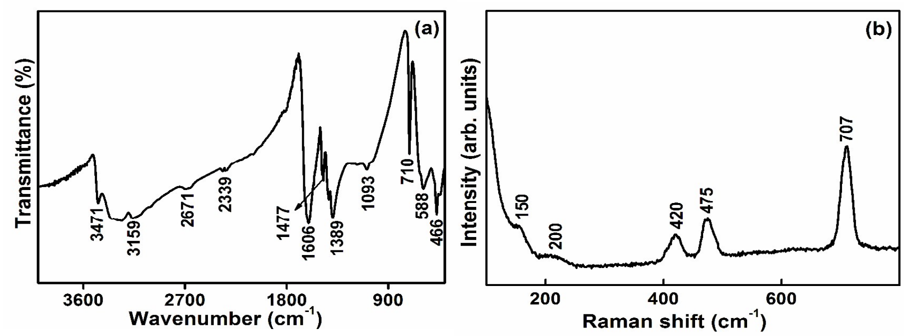

Fig. S1 (a) FT-IR and (b) Raman spectrum of $[Cu(tu)_3]Cl$.

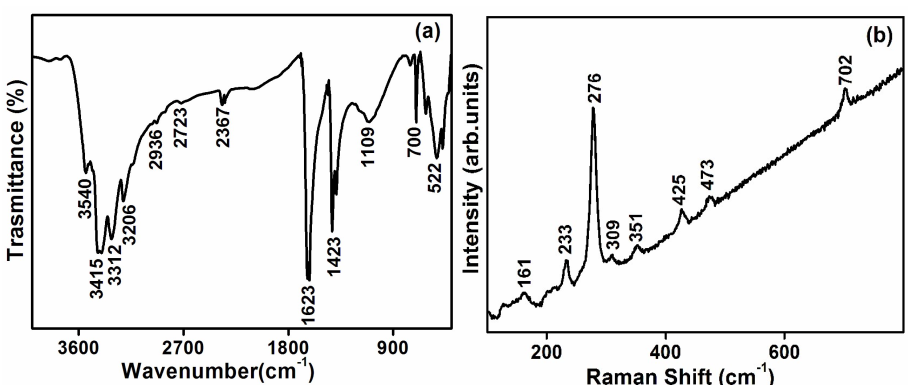

Fig. S2 (a) FT-IR and (b) Raman spectrum of $[Sn(tu)]Cl_2$.

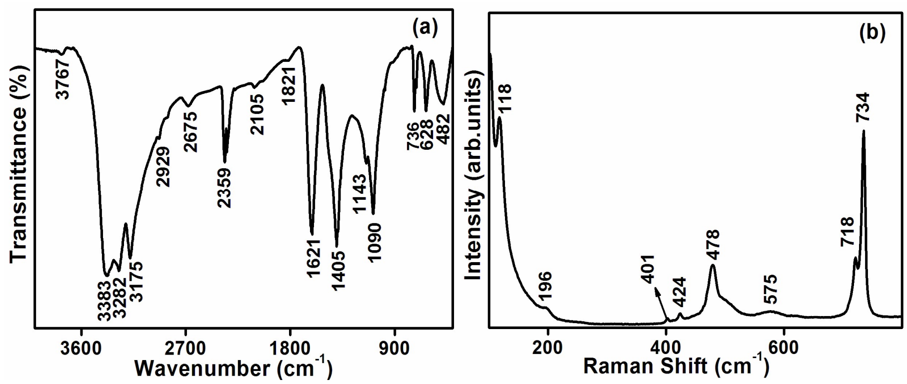

Fig. S3 (a) FT-IR and (b) Raman spectrum of $[Ni(tu)_4]SO_4$.

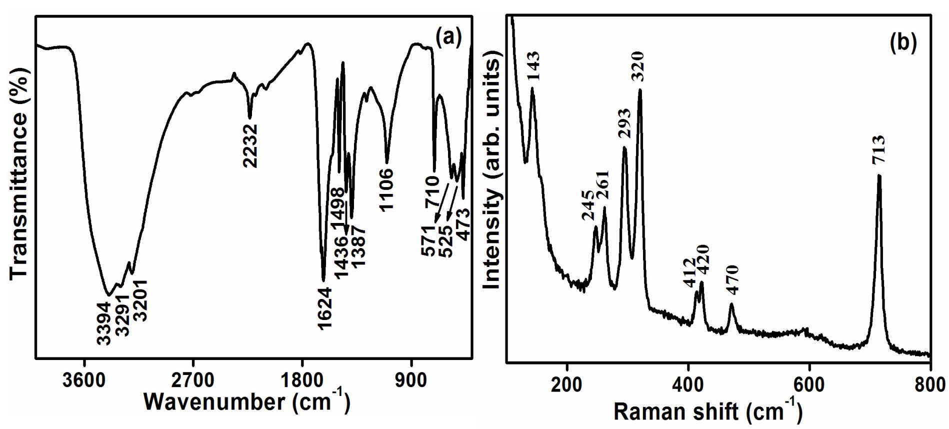

Fig. S4 (a) FT-IR and (b) Raman spectrum of $[Co(tu)_2]Cl_2$.

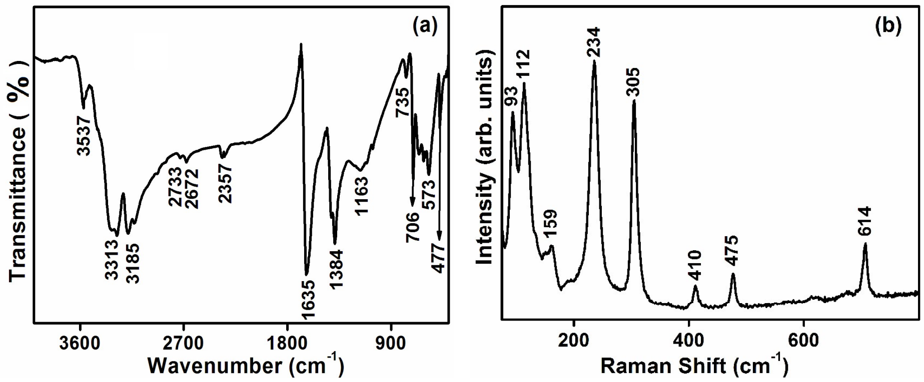

Fig. S5 (a) FT-IR and (b) Raman spectrum of $[Sb(tu)_2]Cl_3$.

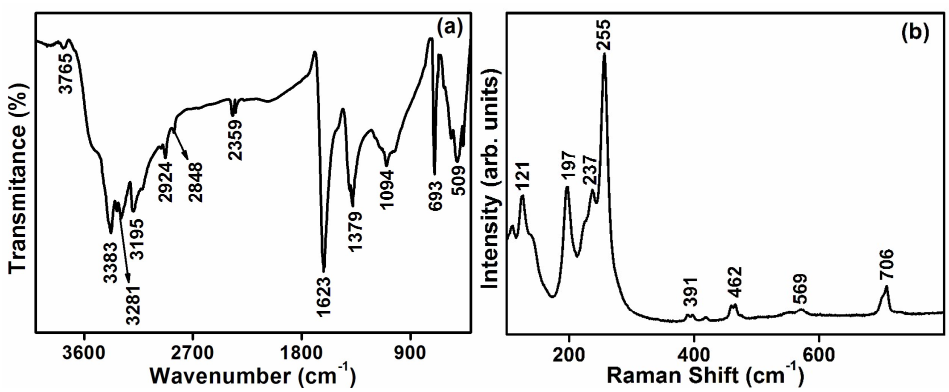

Fig. S6 (a) FT-IR and (b) Raman spectrum of $[Bi_3(tu)_3]Cl_3$.

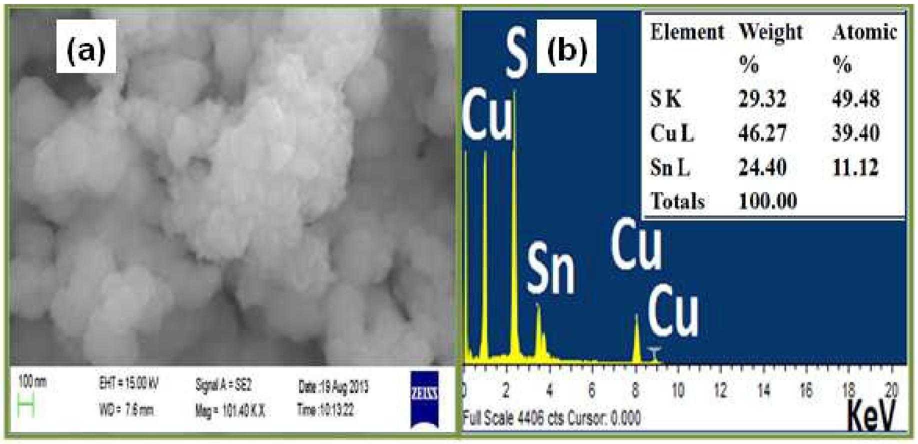

Fig. S7 (a) SEM image and (b) EDX spectrum of Cu_3SnS_4.

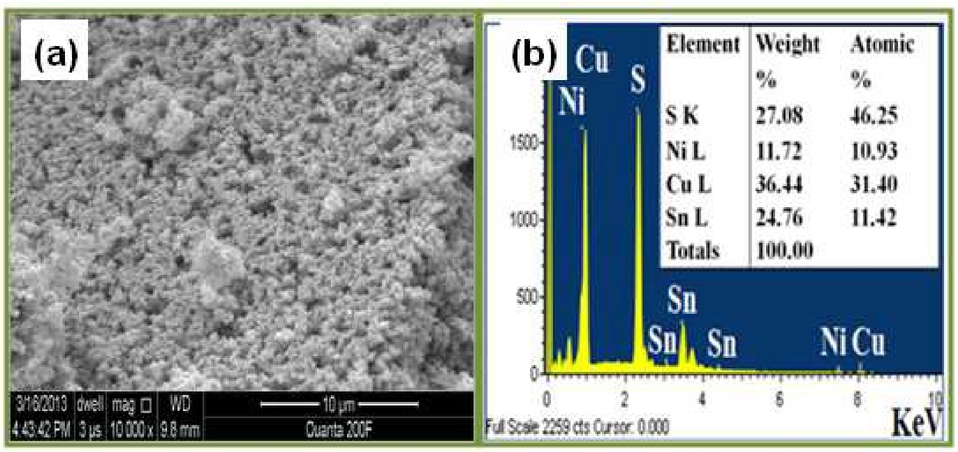

Fig. S8 (a) SEM image and (b) EDX spectrum of product from the attempts to substitute nickel in Cu_3SnS_4.

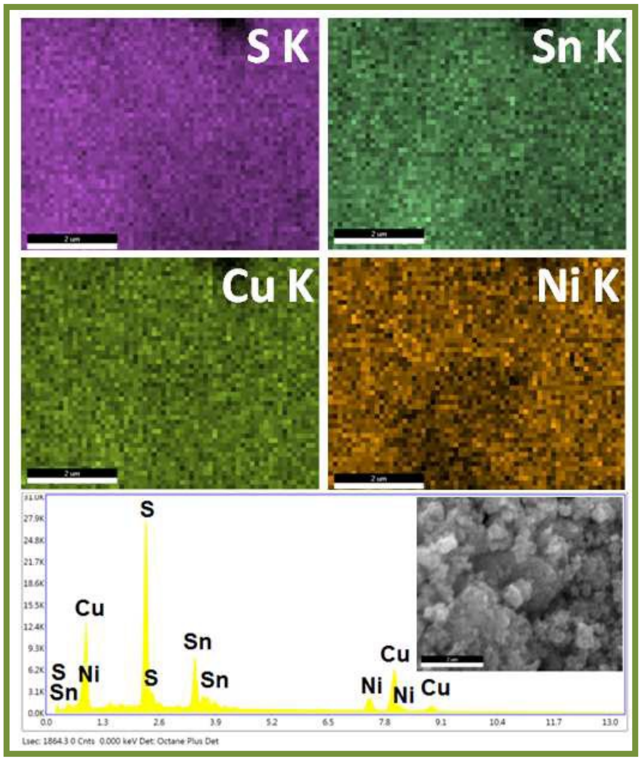

Fig. S9 EDX spectrum and elemental mapping results of Cu_2NiSnS_4.

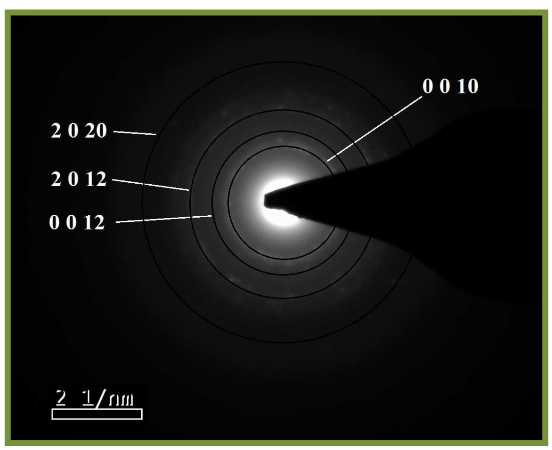

Fig. S10 SAED pattern of Cu_2NiSnS_4.

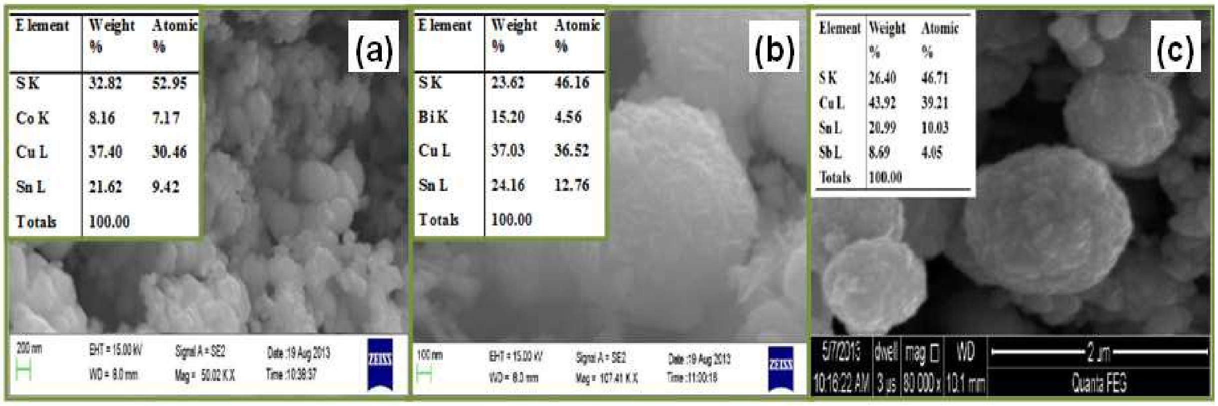

Fig. S11 SEM images with EDX analysis of (a) cobalt (b) bismuth and (c) antimony substituted Cu_3SnS_4 samples.